Phonon-Induced Dephasing of Excitons in Semiconductor Quantum Dots: Multiple Exciton Generation, Fission, and Luminescence

Angeline B. Madrid,[†] Kim Hyeon-Deuk,[†,‡] Bradley F. Habenicht,[†] and Oleg V. Prezhdo[†,*]

[†]Department of Chemistry, University of Washington, Seattle, Washington 98195, and [‡]Department of Chemistry, Kyoto University, Kyoto 606-8502, Japan

ABSTRACT Phonon-induced dephasing processes that govern optical line widths, multiple exciton (ME) generation (MEG), and ME fission (MEF) in semiconductor quantum dots (QDs) are investigated by *ab initio* molecular dynamics simulation. Using Si QDs as an example, we propose that MEF occurs by phonon-induced dephasing and, for the first time, estimate its time scale to be 100 fs. In contrast, luminescence and MEG dephasing times are all sub-10 fs. Generally, dephasing is faster for higher-energy and higher-order excitons and increased temperatures. MEF is slow because it is facilitated only by low-frequency acoustic modes. Luminescence and MEG couple to both acoustic and optical modes of the QD, as well as ligand vibrations. The detailed atomistic simulation of the dephasing processes advances understanding of exciton dynamics in QDs and other nanoscale materials.

KEYWORDS: quantum dots · electron−phonon interaction · multiple excitons · luminescence · dephasing · *ab initio* molecular dynamics · ultrafast

Dynamics of electronic excitations in quantum dots (QDs) made of semiconducting[1,2] and metallic[3] materials underlies a variety of applications, including photovoltaic solar cells,[4−9] light-emitting diodes,[10] field-effect transistors,[11] lasers,[12] quantum emitter antennas,[13] fluorescent biological imaging probes,[14,15] quantum information processing,[16] spintronics,[17] thermopower devices,[18] *etc.* Electron−phonon interactions[19] play key roles in most of these applications and carry significant fundamental and practical importance. For instance, it is desirable in QD lasers that all electrons relax rapidly to the lowest excited state, from which the photons are emitted with an optical gain. Similarly, in biological imaging probes, rapid electron−phonon relaxation to the lowest excited electronic state will generate emission of a well-defined color. In contrast, the decay of the highly excited electrons in QD solar cells results in voltage and current losses, and therefore, it should be avoided.

Electron−phonon interactions give rise to two related but qualitatively different phenomena, namely, relaxation and dephasing. Compared to the electron−phonon energy relaxation, the electron−phonon dephasing is a more subtle effect. An elastic process, the dephasing conserves the electronic energy. It destroys coherences between electronic states, converting them into ensembles of uncorrelated states (Figure 1). Light absorption and emission create superpositions of ground and excited states. Dephasing of such superpositions determines optical line widths. Coulomb interactions generate superpositions of single and multiple excited electron−hole pairs. Elastic dephasing of the exciton superpositions plays a key role in the excited state dynamics in semiconductor QDs, in addition to the relaxation processes that result in energy transfer. As a further step, excitons may dephase into uncorrelated electron−hole pairs that facilitate charge transport.

Particularly exciting is the intense debate regarding the generation of multiexciton (ME) states in semiconductor QDs upon absorption of high-energy photons. Predicted[4] several years before the discovery,[5] ME generation (MEG) from high-energy photons avoids energy losses associated with electron−phonon relaxation to lower energy levels. MEG has drawn close attention due to its potential for significant improvement of photovoltaic device efficiencies.[4−9,20−23,26] First studies of MEG reported extremely high efficiencies.[5−7,20,21,23] Later, MEG yields were shown to depend strongly on the exact conditions of QD synthesis, and the quoted numbers became lower.[20,25−28] Nevertheless, even modest ME yields can provide the fundamental advance that is needed to make the photovoltaic technology into a major resource capable of

*Address correspondence to prezhdo@u.washington.edu.

Received for review February 6, 2009 and accepted August 13, 2009.

Published online September 1, 2009.
10.1021/nn900584p CCC: $40.75

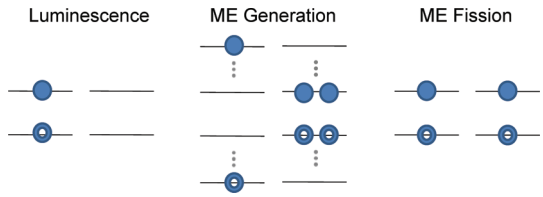

Figure 1. Pairs of states involved in the phonon-induced dephasing processes studied in this work.

competing with the current energy supplies. Detection of MEs in Si QDs[7] is particularly important since the current solar-cell industry is almost entirely Si-based. It is essential that MEs generated in semiconductor QDs can dissociate into free charge carriers and that the free charge carriers can be extracted from the QDs.[8,29,30]

MEG is intimately related to phonon-induced dephasing. Of the three proposed MEG mechanisms, two rely on the dephasing processes. The inverse Auger mechanism of MEG, also known as impact ionization,[4] assumes incoherent transitions from high-energy single-exciton states to MEs. The loss of electronic coherence occurs by coupling to phonons and, in this case, should be faster than MEG. The dephasing mechanism[6,23,31] starts with a coherent superposition of single and ME states and associates MEG with the dephasing of this superposition (Figure 1). In the direct mechanism,[21,22,26] MEs are created immediately upon absorption of a photon. Calculations show[26] that the direct process is particularly efficient in lead salt QDs, in which MEs were seen first,[5,6,23] and that is it quenched by QD charging.[27] Note that, in addition to MEG quenching *per se*, QD charging complicates the analysis of the experimental data and can lead to overestimation of the MEG yields.[25]

Once MEs are created by either mechanism, they must dissociate into uncorrelated excitons (Figure 1) that coexist within the same QD and luminesce independently. The loss of correlation within the coherent superposition of MEs can be named ME fission (MEF) because it is closely related to the singlet fission process in tetracene, anthracene, and other polyacene crystals.[24] Singlet fission in the molecular systems occurs by decay of a photoexcited singlet state into two triplets. It is not clear at present whether MEF produces triplets or singlets in semiconductor QDs. The resulting uncorrelated states emit light. This is possible either if the states are singlets or if they are triplets, and strong spin−orbit coupling allows transitions between triplet and singlet manifolds. The MEF process has not yet been studied in semiconductor QDs. Here, we propose that it occurs by phonon-induced dephasing.

Focusing on a QD made of Si, which is the most important semiconductor, we characterize the phonon-induced dephasing processes for a variety of exciton states at ambient and low temperatures. For the first time, we compute the MEF dephasing time. Additionally, we report the dephasing times that govern optical line widths and MEG. Previously, such values were calculated for PbSe and CdSe QDs.[32,33] In contrast to PbSe and CdSe, Si is an indirect band gap semiconductor. We investigate whether or not the MEG and MEF mechanisms and electron−phonon coupling remain similar in Si. We show that dephasing leading to MEF requires hundreds of femtoseconds. At the same time, dephasing responsible for luminescence line widths and MEG is much quicker, about 10 fs. Generally, dephasing is faster at higher energy, higher temperature, and with higher-order excitons. Both acoustic and optical phonons contribute to luminescence line widths and MEG. The higher-frequency optical modes determine the fast time scales associated with these phenomena. In contrast, MEF is facilitated only by low-frequency acoustic modes. As a result, it proceeds slowly and varies with temperature more than MEG and luminescence.

RESULTS AND DISCUSSION

The vibrationally induced dephasing times for MEG, MEF, and luminescence line width are computed using the optical response function formalism,[34] as described in the Methods section, eqs 1−6. The calculations are performed with the $Si_{29}H_{24}$ QD presented in Figure 2a.

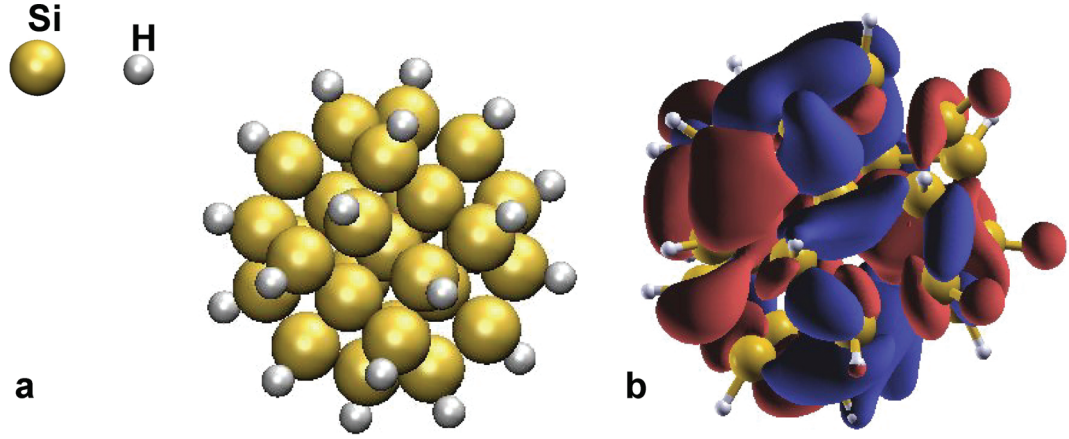

Figure 2. (a) Optimized geometry of $Si_{29}H_{24}$ quantum dot. (b) Band gap transition density. Red and blue colors correspond to positive and negative density changes.

The exciton, biexciton, and triexciton states were represented in the Kohn−Sham orbital picture by promoting one, two, and three electrons from occupied to unoccupied orbitals, respectively. As an example, Figure 2b shows the transition density for the lowest-energy electronic excitation. The density has a complicated structure but is mostly localized on the Si atoms, indicating that hydrogens do a good job terminating the dangling bonds. The excitation energies were estimated from the orbital energies and their occupation numbers. This approximate, but computationally efficient, treatment of electronic excitations was essential in order to achieve statistical convergence of the optical response functions, requiring thousands of electronic structure calculations.

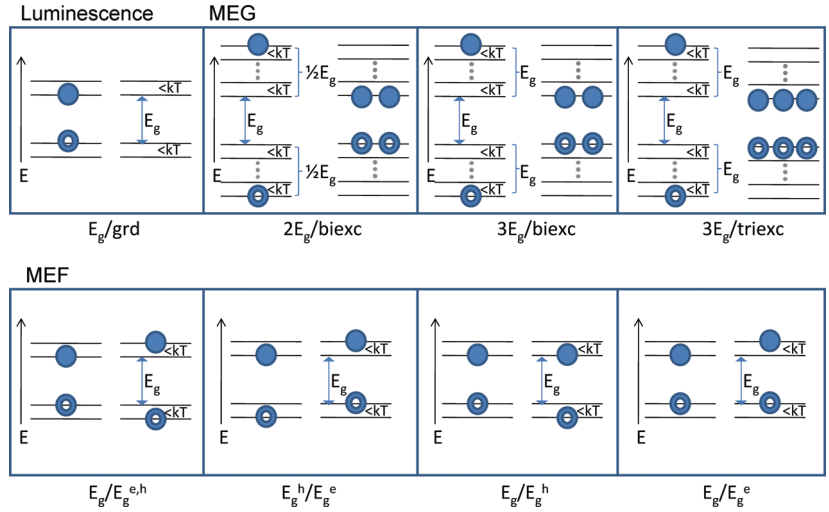

Figure 3. Detailed diagram of the dephasing processes considered here. The corresponding dephasing time scales are given in Table 1. Top row: dephasing of the superposition between the band gap exciton (E_g) and ground state determines the luminescence line width; MEG involves dephasing of single and multiple excitons, such as the double band gap exciton and biexciton ($2E_g$/biexc), the triple band gap exciton and triexciton ($3E_g$/triexc), and off-resonant superposition of the triple band gap exciton and biexciton ($3E_g$/biexc). Bottom row: MEF involves dephasing of various superpositions of single excitons within k_BT of the band gap.

Figure 3 provides a detailed diagram of the dephasing processes under consideration. The corresponding dephasing times are presented in Table 1. The two states shown in each frame in Figure 3 are in a coherent superposition initially. The superposition dephases due to electron−phonon coupling. Dephasing of the superposition between the band gap excited state E_g and the ground state determines the luminescence line width, which can be directly compared to experimental data.[35] The rest of the top row shows three examples of superpositions of single and MEs: a $2E_g$ single exciton that is near-resonant in energy with the band gap biexciton, a $3E_g$ single exciton with the band gap biexciton, and the $3E_g$ single exciton that is near-resonant with the band gap triexciton.

Note that the energies of the states in the $3E_g$/biexciton superposition are different, in contrast to the $2E_g$/biexciton and $3E_g$/triexciton superpositions. The $3E_g$/biexciton superposition is possible quantum mechanically. After the dephasing, the system becomes a statistical mixture of the $3E_g$ and biexciton states. Experimentally, this implies, for example, that 100 photons of energy $2.5E_g$ will produce, after the dephasing, 50 $3E_g$ states and 50 biexcitons. If only a single photon is absorbed, there will be a 50% chance to observe the $3E_g$ state and a 50% chance to observe the biexciton. The energy conservation law will not be violated because measuring a state energy requires interaction with the quantum system. The $0.5E_g$ energy difference between the $2.5E_g$ energy of the photon and either the $3E_g$ or biexciton energy will be accommodated by the measuring apparatus.

The diagrams in Figure 3 are schematic. For instance, three electrons and holes forming a triexciton cannot occupy only two orbitals. In reality, the particles reside over a range of orbitals within k_BT of energy, creating ensembles of bi- and triexcitons.

The bottom row in Figure 3 depicts the biexciton fission diagrams. In the orbital picture adopted here, electrons and holes occupy orbitals that are delocalized over the whole QD. The number of orbitals is large, and the energy spacing between them is small, on the order of k_BT. The E_g exciton is a collection of excitons occupying orbitals near the band gap. In order for a ME to dephase, the resulting single excitons must be distinct in some way. Otherwise, their coupling to phonons will be identical and no dephasing can occur. Therefore, we consider MEF into single excitons that have different occupations of the orbitals within k_BT near the band gap. Four possibilities are considered. The first and second diagrams in the bottom row of Figure 3 involve symmetric and asymmetric differences in both electron and hole occupations. The third and fourth diagrams involve changes in either hole or electron occupation.

TABLE 1. Dephasing Times (fs) for All Processes Shown in Figure 3

process		$T = 80$ K $\langle E_g \rangle = 2.55$ eV	$T = 300$ K $\langle E_g \rangle = 2.34$ eV
luminescence	E_g/grd	6.98 ± 0.21	3.96 ± 0.10
MEG	$2E_g$/biexc	7.33 ± 0.17	3.95 ± 0.13
	$3E_g$/biexc	4.88 ± 0.11	2.63 ± 0.07
	$3E_g$/triexc	2.96 ± 0.09	1.60 ± 0.05
MEF	$E_g/E_g^{e,h}$	205.33 ± 0.87	54.43 ± 1.06
	E_g^h/E_g^e	334.78 ± 5.29	86.25 ± 1.58
	E_g/E_g^h	337.52 ± 3.02	103.14 ± 1.63
	E_g/E_g^e	367.01 ± 1.94	78.73 ± 0.96

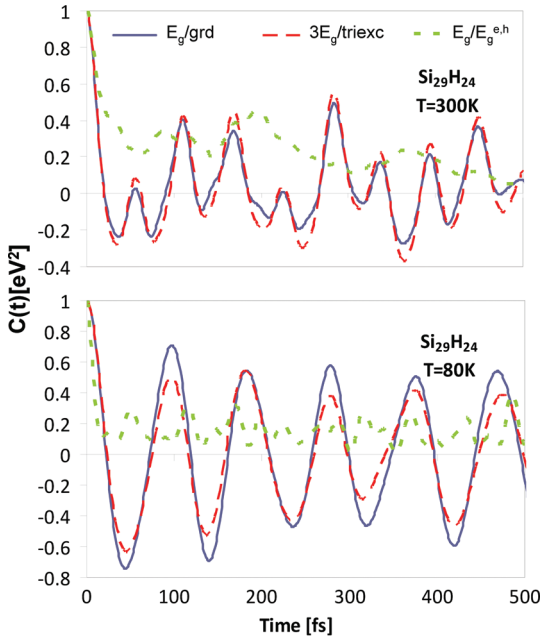

Figure 4. ACFs for the luminescence (E_g/grd), MEG ($3E_g$/triexc), and MEF ($E_g/E_g^{e,h}$) dephasing processes defined in Figure 3. The top and bottom frames correspond to ambient and low temperatures as indicated. The luminescence and MEG ACFs differ from MEF ACFs because MEF couples to a different set of phonons (Figure 5).

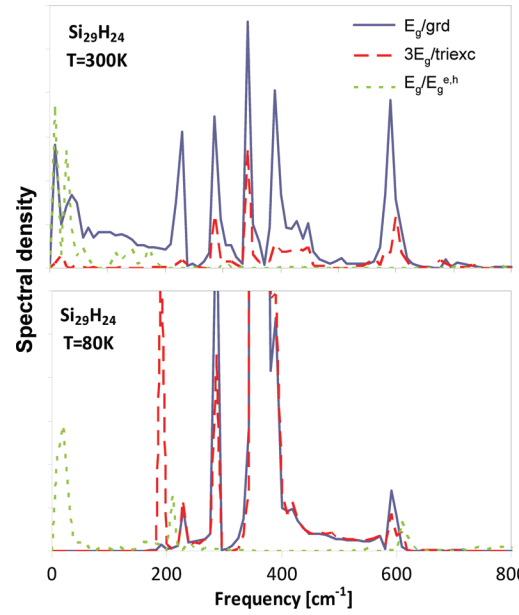

Figure 5. Fourier transforms of ACFs shown in Figure 4.

The optical response functions characterizing the dephasing processes can be obtained directly or *via* the second-order cumulant expansion;[34] see detailed discussion in the Methods section. Both cumulant (eq 5) and direct (eq 6) approaches give similar results, and only the direct dephasing data will be discussed below. However, the cumulant approximation involves intermediate steps and provides additional insights into the dephasing process. Figure 4 presents the normalized autocorrelation functions (ACFs), defined in eq 3, for the luminescence (E_g/ground), MEG ($3E_g$/triexciton), and MEF ($E_g/E_g^{e,h}$) processes at 300 and 80 K. The first two ACFs track each other quite closely. In contrast, the ACFs describing MEF oscillate with much smaller amplitudes. Since the higher temperature excites a wider range of vibrations and makes them less harmonic, the ACFs oscillate more randomly at 300 than at 80 K. Defects expand the frequency range and increase anharmonicity, speeding up ACF decay as seen, for instance, in carbon nanotubes.[36] Thermally induced surface deformations and terminating hydrogen atoms could be viewed as defects in the present case. Indeed, as shown in Figure 2b, the band gap transition density extends onto a few hydrogen atoms on the Si QD surface.

The Fourier transforms (FT) of the ACFs (eq 4) are shown in Figure 5. They indicate that both acoustic and optical modes contribute to luminescence line widths and MEG. As with the ACFs (Figure 4), the E_g/ground and $3E_g$/triexciton data closely match. In contrast, only low-frequency acoustic modes are involved in MEF. It should be noted that quantum confinement induces mixing of different types of modes,[37] and phonons can be classified as acoustic or optical only approximately. The majority of the modes contributing to the dephasing processes involved in luminescence and MEG lie within the 200−500 cm^{-1} frequency range. Further peaks appear at 600 cm^{-1} and at the very low frequencies of less than 100 cm^{-1}. The phonon around 350−360 cm^{-1}, seen in the vibrational density of states in Si QDs,[37] is particularly important, especially at the lower temperature (bottom panel of Figure 5). Thermal fluctuations break the symmetry of the QD and distort its geometry. As a result, a larger number of modes contribute to the luminescence and MEG dephasing processes at the higher temperature. This can be seen particularly well with the low-frequency modes, which appear only at $T = 300$ K and arise due to QD distortions. Compared to the PbSe and CdSe QDs of similar size,[32,33] dephasing of luminescence and MEG is caused by higher-frequency modes in the Si QD, as should be expected, since Si is a lighter atom. MEF is dominated by low frequencies at both temperatures. MEF involves orbitals that are close in energy (see Figure 3) and, therefore, have similar densities, number of nodes, *etc.* As a result, the energy gaps between pairs of low-energy excitons oscillate very slowly, even though the energies of individual excitons oscillate fast, as evidenced by the E_g/ground data.

The direct dephasing functions (eq 6), corresponding to Figures 4 and 5, are plotted in Figure 6. The dephasing times shown in Table 1 for all processes specified in Figure 3 were obtained by fitting the dephasing functions with Gaussians. The dephasing times involved in luminescence and MEG are all sub-10 fs. The dephasing involving a triexciton occurs faster than the dephasing involving a biexciton or a single exciton.

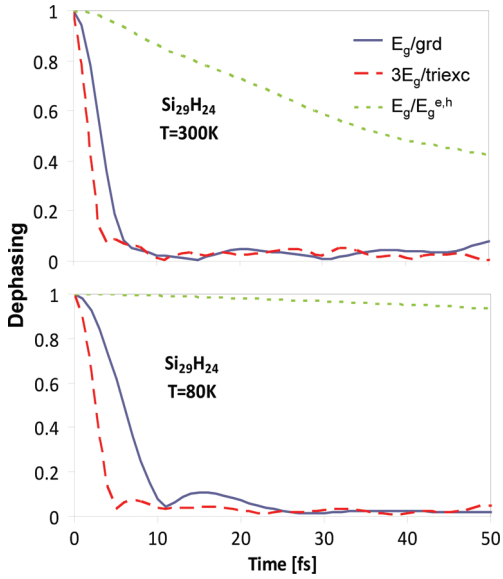

Figure 6. Dephasing functions for the luminescence, MEG and MEF processes considered in Figures 4 and 5. Dephasing times obtained by Gaussian fitting are shown in Table 1.

The dephasing of MEF is significantly slower than dephasing responsible for luminescence line widths and MEG. The order of magnitude difference becomes more pronounced at the lower temperature. The drastic disparity in the decays of the dephasing functions shown in Figure 6 contradicts, at the first glance, the similarity of the ACF decay rates (Figure 4). In the cumulant approximation (eq 5), the dephasing rate can be attributed to a combination of decay time and amplitude of un-normalized ACF. It is the amplitude that is responsible for the large difference between the dephasing times of MEF and MEG/luminescence. The fluctuation of the MEG and luminescence energy gaps determines the initial value of the unnormalized ACF (eq 2). Larger gap fluctuations convert to faster dephasing. The states involved in MEF are very close in energies (Figure 3). The state densities are similar, and the energy gaps between these states fluctuate little. Density changes involved in MEG and luminescence create more significant perturbations to the vibrational lattice, involve a broader range of phonon motions (Figure 5), and accelerate dephasing (Figure 6 and Table 1). Since the MEF dephasing times arise from small fluctuations of the energy gaps, they should be sensitive to QD size, surface ligands, solvent, *etc*. Nevertheless, it is quite clear that, generally, MEF dephasing should take much longer than that of MEG and luminescence. While the MEF time has not been measured yet in semiconductor QDs, the MEF time calculated here for Si QD agrees with the time scale of singlet fission observed in molecular systems.[38]

The loss of coherence between the ground and the lowest excited state is ultrafast, and therefore, the homogeneous widths of luminescence lines in isolated Si QDs should be remarkably broad. The line widths deduced from the present theory are about 150 meV at room temperature and 80 meV at 80 K, in agreement with the available experimental data.[39,40] The experimental values are somewhat smaller, 130 and 60 meV, correspondingly, since they were measured using significantly larger Si nanoclusters. Note that the current results correspond to the overall shape of the emission line. The ultra-narrow peaks observed at the lower temperature[40] are attributed to individual phonon modes. The line widths reported here include contributions from all phonon modes.

The luminescence and MEG dephasing times computed for the Si QD are very similar to those obtained previously for a range of PbSe and CdSe QDs.[32,33] Even though Si is an indirect band gap semiconductor, in contrast to PbSe and CdSe, this qualitative difference disappears for small QDs. Recent experiments show that small Si QDs with quantum confinement energies greater than 1 eV and sizes less than 4 nm behave similarly to the direct gap QDs.[41]

The Kohn−Sham density functional theory formalism used here captures some of the electron correlation effects, which enter implicitly through the functional. However, more advanced theories are needed for description of strong excitonic effects.[22,26] The excitonic interactions should be more important in Si and CdSe QDs than in PbSe because the bulk dielectric constants of Si[42] and CdSe[43] are small, 11.97 and 6.2, respectively, compared to 250 for PbSe,[43] and the screening of excitonic interactions is not as effective. Additionally, the exciton radius of bulk Si is relatively small,[44] 4.3 nm, compared to 46 and 6 nm for PbSe and CdSe.[45] Therefore, the electron kinetic energy associated with quantum confinement starts dominating over the excitonic interactions at a smaller QD size in Si than in PbSe. Quantum confinement dominates excitonic interactions in the small Si QD considered here. However, in larger dots, one can anticipate a change in the cluster size dependence of the dephasing rate[46] and in the difference among the exciton/biexciton/triexciton dephasing times.[47] Estimating the effect of strong excitonic interactions on the dephasing dynamics in Si QDs remains an open question.

CONCLUSIONS

The current study proposes that MEF occurs by dephasing of a coherent ME superposition due to coupling to phonons. The established MEF time scale, 50−400 fs depending on temperature and biexciton type, agrees with the available experimental data.[38] The larger the difference in the nature of the two excitons creating the biexciton, the faster the fission: compare the $E_g/E_g^{e,h}$ case with the other three possibilities (Figure 3 and Table 1). In larger dots, the spacing of the energy levels near the band gap will decrease, and the excitons creating MEs will occupy states that are more similar in nature. This factor will extend the MEF

dephasing process. At the same time, the denser set of phonon modes and surface defects that are more likely in larger dots should accelerate dephasing.[43,48] Surface ligands and solvents can create additional dephasing pathways, as well.[7,49−51] It is likely that the phonon dephasing mechanism of MEF acts in both QD and molecular systems.[24,38,52]

The conclusions obtained for the MEG process with the current Si QD simulation agree with the earlier results for the PbSe and CdSe QDs.[32,33] According to the calculations, the MEG dephasing time is on the order of 10 fs. The ultrafast dephasing suggests that impact ionization described by rate expressions[4] is one of the key MEG mechanisms. The fact that biexcitons and triexcitons dephase faster than single excitons supports the dephasing mechanism of MEG.[6,23] The short but finite coherence time is sufficient for direct photogeneration of multiple excitons,[21,26] provided that the Coulomb interaction that mixes the single and multi-exciton states is on the order of tens of electron volts or stronger. The dephasing parameters obtained here provide valuable input to the phenomenological models.[6,53]

In summary, we proposed a dephasing mechanism for the MEF process in semiconductor QDs. The 100 fs MEF time scale was estimated for the first time and agrees with the available experimental data.[38] Additionally, we reported the first atomistic calculation of the pure dephasing contribution to the luminescence line widths of Si QDs, rationalizing the experiments.[39,40] The sub-10 fs MEG dephasing times evaluated for the Si QD are similar to the earlier calculations for PbSe and CdSe QDs.[32,33] The dephasing time scales of MEF are much longer than those of MEG and luminescence due to small differences in the nature of excitons involved in MEF relative to MEG and luminescence. For the same reason, the MEF process is facilitated by low-frequency acoustic modes, while both acoustic and optical modes contribute to MEG and luminescence line widths. Since the dynamics of the lower-frequency modes is more significantly affected by temperature variations, the MEF dephasing time shows stronger temperature dependence than the other two dephasing times. Therefore, the large difference in the dephasing time scales for the MEF and MEG processes is emphasized at lower temperatures.

Surface modes involving the terminating hydrogen atoms and a layer of silicon atoms play important roles in the dephasing processes involved in luminescence and MEG. The properties of these modes should be roughly independent of the cluster size. A slight frequency red shift can be expected in larger clusters due to stronger mixing with the lower-frequency bulk modes. The contribution of the surface modes to the dephasing processes relative to the bulk modes should decrease with increasing cluster size. Further studies of the surface modes are underway.

The results reported here provide valuable insights into the dynamics of excited electronic states in semiconductor QDs and contribute to our understanding of the role of MEs in the efficiencies of photovoltaic devices.

METHODS

The vibrationally induced dephasing times for MEG, MEF, and luminescence line width are computed using the optical response function formalism.[34] Excluding inhomogeneous broadening associated with a distribution of optically active species, the intrinsic homogeneous line width, Γ, of an optical transition is inversely proportional to the dephasing time T_2. The latter includes the excited state lifetime T_1 and pure dephasing time T_2^*:

$$\Gamma = \frac{1}{T_2} = \frac{1}{2T_1} + \frac{1}{T_2^*} \quad (1)$$

For sufficiently long T_1, Γ is determined by T_2^*.

The pure dephasing time is associated with fluctuations of the energy levels due to coupling of electrons to phonons of the semiconductor, ligands, a solvent, *etc*. The fluctuations in the energy levels are best characterized in terms of correlation functions. The un-normalized autocorrelation function (ACF) for a transition of energy E is defined as

$$C_u(t) = \langle \Delta E(t) \Delta E(0) \rangle \quad (2)$$

where $\Delta E = E - \langle E \rangle$, and the angular brackets denote averaging over a statistical ensemble, in particular, canonical averaging in the present study. The initial value of the un-normalized ACF gives the average fluctuation in the transition energy, $C_u(0) = \langle \Delta E^2(0) \rangle$. Dividing $C_u(t)$ by $C_u(0)$ gives the normalized ACF:

$$C(t) = \frac{\langle \Delta E(t) \Delta E(0) \rangle}{\langle \Delta E^2(0) \rangle} \quad (3)$$

ACFs characterize periodicity and memory of the energy fluctuations. Rapid decay of an ACF indicates short memory and occurs if multiple phonon modes couple to the electronic transition and if the coupling is anharmonic.

The Fourier transform (FT) of the ACF is known as the spectral density:

$$I(\omega) = \left| \frac{1}{\sqrt{2\pi}} \int_{-\infty}^{\infty} dt\, e^{-i\omega t} C(t) \right|^2 \quad (4)$$

It identifies the frequencies of those phonon modes that efficiently couple to the electronic subsystem. The strength of the electron−phonon coupling for a particular mode is related to the intensity of the corresponding line in the spectral density.

The optical response functions characterizing the dephasing processes for a pair of states that are entangled in a coherent superposition can be obtained directly or *via* the second-order cumulant expansion.[34] The cumulant expansion approximation involves the ACF that, together with its FT, provides additional information about the dephasing process. The cumulant dephasing function is obtained by double integration and exponentiation of the unnormalized ACF (eq 2).

$$D(t) = \exp(-g(t)), \quad g(t) = \frac{1}{\hbar^2} \int_0^t d\tau_1 \int_0^{\tau_1} d\tau_2\, C_u(\tau_2) \quad (5)$$

The above expression indicates that rapid dephasing is facilitated by a large fluctuation of the transition energy, that is, large $C_u(0) = \langle \Delta E^2(0) \rangle$, as well as by a short memory of the fluctuation (*i.e.*, rapidly decaying ACF).

Alternatively, the dephasing function can be computed directly as

$$D(t) = \exp(i\omega t)\left\langle \exp\left(-\frac{i}{\hbar}\int_0^t \Delta E(\tau)\, d\tau\right)\right\rangle \quad (6)$$

Here, ω is the thermally averaged transition energy $\langle \Delta E \rangle$ divided by $\hbar$. The direct expression is more difficult to converge because it involves averaging of a complex-valued oscillatory function

$$\exp\left(-\frac{i}{\hbar}\int_0^t \Delta E(\tau)\, d\tau\right)$$

whose real and imaginary parts change signs. In comparison, the cumulant expression (eqs 2 and 5) involves averaging of a real and positively valued transition energy and its ACF.

The phonon-induced dephasing of electronic transitions of molecular chromophores is often characterized at the atomistic level by molecular dynamics (MD) simulations.[54] Phenomenological models developed for crystals[55] clarify trends associated with crystal size, electron−phonon coupling strength, temperature, *etc*.

The atomistic calculations reported here were performed with the $Si_{29}H_{24}$ QD. The initial geometry of the cluster was generated from Si bulk structure. Hydrogen atoms were added in order to terminate the dangling Si bonds and eliminate spurious surface states. The geometry of the cluster was fully optimized at zero temperature. The cluster was brought up to 80 and 300 K by MD with repeated velocity rescaling. Microcanonical trajectories of 5 ps duration were produced for each temperature using the Verlet algorithm with a 1 fs time step and Hellman−Feynman forces. The relaxed $Si_{29}H_{24}$ cluster shown in Figure 2a preserved the bulk topology of Si. The dynamics involved no major changes in the QD atomic and electronic structure, such as bond breaking, and the 5 ps trajectories provided converged results. The convergence was tested by computing the statistical averages over shorter trajectories. The qualitative trends were preserved, and the quantitative differences were less than 10%. The simulations were performed using density functional theory implemented with the Vienna *Ab Initio* Simulation Package.[56] The projector-augmented-wave pseudopoteintals, Perdew−Wang 91 generalized-gradient density functional,[57] and a converged plane-wave basis set were employed.

Acknowledgment. A.B.M. and O.V.P. acknowledge financial support of DOE (Grant No. DE-FG02-05ER15755) and ACS PRF (Grant No. 41436-AC6). K.H.D. is partially supported by Grants-in-Aid for Scientific Research from Japan Society for the Promotion of Science (Grant No. 17740278) and by the Global COE Program "Integrated Materials Science" (#B-09).

REFERENCES AND NOTES

1. Milliron, D. J.; Hughes, S. M.; Cui, Y.; Manna, L.; Li, J. B.; Wang, L. W.; Alivisatos, A. P. Colloidal Nanocrystal Heterostructures with Linear and Branched Topology. *Nature* **2004**, *430*, 190–195.
2. Peterson, J. J.; Huang, L.; Delerue, C.; Allan, G.; Krauss, T. D. Uncovering Forbidden Optical Transitions in PbSe Nanocrystals. *Nano Lett.* **2007**, *7*, 3827–3831.
3. Lindberg, V.; Hellsing, B. Metallic Quantum Dots. *J. Phys.: Condens. Matter* **2005**, *17*, S1075–S1094.
4. Nozik, A. J. Spectroscopy and Hole Electron Relaxation Dynamics in Semiconductor Quantum Wells and Quantum Dots. *Annu. Rev. Phys. Chem.* **2001**, *52*, 193–231.
5. Schaller, R. D.; Klimov, V. I. High Efficiency Carrier Multiplication in PbSe Nanocrystals: Implications for Solar Energy Conversion. *Phys. Rev. Lett.* **2004**, *92*, 186601-1–18660-4.
6. Ellingson, R. J.; Beard, M. C.; Johnson, J. C.; Yu, P.; Micic, O. I.; Nozik, A. J.; Shabaev, A.; Efros, A. L. Highly Efficient Multiple Exciton Generation in Colloidal PbSe and PbS Quantum Dots. *Nano Lett.* **2005**, *5*, 865–871.
7. Beard, M. C.; Knutsen, K. P.; Yu, P.; Luther, J. M.; Song, Q.; Metzger, W. K.; Ellingson, R. J.; Nozik, A. J. Multiple Exciton Generation in Colloidal Silicon Nanocrystals. *Nano Lett.* **2007**, *7*, 2506–2512.
8. Hyun, B. R.; Zhong, Y. W.; Bartnik, A. C.; Sun, L. F.; Abruna, H. D.; Wise, F. W.; Goodreau, J. D.; Matthews, J. R.; Leslie, T. M.; Borrelli, N. F. Electron Injection from Colloidal PbS Quantum Dots into Titanium Dioxide Nanoparticles. *ACS Nano* **2008**, *2*, 2206–2212.
9. Koleilat, G. I.; Levina, L.; Shukla, H.; Myrskog, S. H.; Hinds, S.; Pattantyus-Abraham, A. G.; Sargent, E. H. Efficient, Stable Infrared Photovoltaics Based on Solution-Cast Colloidal Quantum Dots. *ACS Nano* **2008**, *2*, 833–840.
10. Coe, S.; Woo, W.; Bawendi, M.; Bulovic, V. Electroluminescence from Single Monolayers of Nanocrystals in Molecular Organic Devices. *Nature* **2002**, *420*, 800–803.
11. Talapin, D. V.; Murray, C. B. PbSe Nanocrystal Solids for n- and p-Channel Thin Film Field-Effect Transistors. *Science* **2005**, *310*, 86–89.
12. Klimov, V. I.; Mikhailovsky, A. A.; Xu, S.; Malko, A.; Hollingsworth, J. A.; Leatherdale, C. A.; Eisler, H. J.; Bawendi, M. G. Optical Gain and Stimulated Emission in Nanocrystal Quantum Dots. *Science* **2000**, *290*, 314–317.
13. Farahani, J.; Pohl, D.; Eisler, H.; Hecht, B. Single Quantum Dot Coupled to a Scanning Optical Antenna: A Tunable Superemitter. *Phys. Rev. Lett.* **2005**, *95*, 017402-1017402−4.
14. Dahan, M.; Levi, S.; Luccardini, C.; Rostaing, P.; Riveau, B.; Triller, A. Diffusion Dynamics of Glycine Receptors Revealed by Single-Quantum Dot Tracking. *Science* **2003**, *302*, 442–445.
15. Evans, C. M.; Guo, L.; Peterson, J. J.; Maccagnano-Zacher, S.; Krauss, T. D. Ultrabright PbSe Magic-Sized Clusters. *Nano Lett.* **2008**, *8*, 2896–2899.
16. Petta, J. R.; Johnson, A. C.; Taylor, J. M.; Laird, E. A.; Yacoby, A.; Lukin, M. D.; Marcus, C. M.; Hanson, M. P.; Gossard, A. C. Coherent Manipulation of Coupled Electron Spins in Semiconductor Quantum Dots. *Science* **2005**, *309*, 2180–2184. Scholz, M.; Aichele, T.; Ramelow, S.; Benson, O. Deutsch-Jozsa Algorithm Using Triggered Single Photons from a Single Quantum Dot. *Phys. Rev. Lett.* **2006**, *96*, 180501-1–180501-4.
17. Berezovsky, J.; Mikkelsen, M. H.; Stoltz, N. G.; Coldren, L. A.; Awschalom, D. D. Picosecond Coherent Optical Manipulation of a Single Electron Spin in a Quantum Dot. *Science* **2008**, *320*, 349–352.
18. Scheibner, R.; Buhmann, H.; Reuter, D.; Kiselev, M.; Molenkamp, L. Thermopower of a Kondo Spin-Correlated Quantum Dot. *Phys. Rev. Lett.* **2005**, *95*, 176602-1–176602-4.
19. Kilina, S. V.; Kilin, D. S.; Prezhdo, O. V. Breaking the Phonon Bottleneck in PbSe and CdSe Quantum Dots: Time-Domain Density Functional Theory of Charge Carrier Relaxation. *ACS Nano* **2009**, *3*, 93–99.
20. Rabani, E.; Baer, R. Distribution of Multiexciton Generation Rates in CdSe and InAs Nanocrystals. *Nano Lett.* **2008**, *8*, 4488–4492.
21. Schaller, R. D.; Sykora, M.; Pietryga, J. M.; Klimov, V. I. Seven Exciton at a Cost of One: Redefining the Limits for Conversion Efficiency of Photons into Charge Carriers. *Nano Lett.* **2006**, *6*, 424–429. Schaller, R. D.; Agranovich, V. M.; Klimov, V. I. High-Efficiency Carrier Multiplication Through Direct Photogeneration of Multi-Excitons *via* Virtual Single-Exciton States. *Nat. Phys.* **2005**, *1*, 189–194.
22. Prezhdo, O. V. Multiple Excitons and the Electron-Phonon Bottleneck in Semiconductor Quantum Dots: An *Ab Initio* Perspective. *Chem. Phys. Lett.* **2008**, *460*, 1–9.
23. Murphy, J. E.; Beard, M. C.; Norman, A. G.; Ahrenkiel, S. P.; Johnson, J. C.; Yu, P.; Mićić, O. I.; Ellingson, R. J.; Nozik, A. J. PbTe Colloidal Nanocrystals: Synthesis, Characterization, and Multiple Exciton Generation. *J. Am. Chem.Soc.* **2006**, *128*, 3241–3247.
24. Hanna, M. C.; Nozik, A. J. Solar Conversion Efficiency of Photovoltaic and Photoelectrolysis Cells with Carrier

Multiplication Absorbers. *J. Appl. Phys.* **2006**, *100*, 074510-1–074510-8.
25. Nair, G.; Bawendi, M. G. Carrier Multiplication Yields of CdSe and CdTe Nanocrystals by Transient Photoluminescence Spectroscopy. *Phys. Rev. B* **2007**, *76*, 081304. Nair, G.; Geyer, S. M.; Chang, L.-Y.; Bawendi, M. G. Carrier Multiplication Yields PbS and PbSe Nanocrystals Measured by Transient Photoluminescence. *Phys. Rev. B* **2008**, *78*, 125325-1–125325-10.
26. Isborn, M. C.; Kilina, S. V.; Li, X.; Prezhdo, O. V. Generation of Multiple Excitons in PbSe and CdSe Quantum Dots by Direct Photoexcitation: First-Principles Calculations on Small PbSe and CdSe Clusters. *J. Phys. Chem. C* **2008**, *112*, 18291–18294.
27. Isborn, C. M.; Prezhdo, O. V. Charging Quenches Multiple Exciton Generation in Semiconductor Nanocrystals: First-Principles Calculations on Small PbSe Clusters. *J. Phys. Chem. C* **2009**, *113*, 12617–12621.
28. Beard, M. C.; Midgett, A. G.; Law, M.; Semonin, O. E.; Ellingson, R. J.; Nozik, A. J. Variations in the Quantum Efficiency of Multiple Exciton Generation for a Series of Chemically Treated PbSe Nanocrystal Films. *Nano Lett.* **2009**, *9*, 836–845.
29. Scholes, G. D. Insights into Excitons Confined to Nanoscale Systems: Electron−Hole Interaction, Binding Energy, and Photodissociation. *ACS Nano* **2008**, *2*, 523–537.
30. Luther, J. M.; Law, M.; Beard, M. C.; Song, Q.; Reese, M. O.; Ellingson, R. J.; Nozik, A. J. Schottky Solar Cells Based on Colloidal Nanocrystal Films. *Nano Lett.* **2008**, *8*, 3488–3492.
31. Shabaev, A.; Efros, A. I.; Nozik, A. J. Multiexciton Generation by a Single Photon in Nanocrystals. *Nano Lett.* **2006**, *6*, 2856–2863.
32. Kamisaka, H.; Kilina, S. V.; Yamashita, K.; Prezhdo, O. V. Ultrafast Vibrationally-Induced Dephasing of Electronic Excitations in PbSe. *Nano Lett.* **2006**, *6*, 2295–2300.
33. Kamisaka, H.; Kilina, S. V.; Yamashita, K.; Prezhdo, O. V. Ultrafast Vibrationally-Induced Dephasing of Electronic Excitations in PbSe Quantum Dots. *J. Phys. Chem. C* **2008**, *112*, 7800–7808.
34. Mukamel, S. *Principles of Nonlinear Optical Spectroscopy*; Oxford University Press: New York, 1995.
35. Peterson, J. J.; Krauss, T. D. Fluorescence Spectroscopy of Single Lead Sulfide Quantum Dots. *Nano Lett.* **2006**, *6*, 510–514.
36. Habenicht, B. F.; Kamisaka, H.; Yamashita, K.; Prezhdo, O. V. *Ab Initio* Study of Vibrational Dephasing of Electronic Excitations in Semiconducting Carbon Nanotubes. *Nano Lett.* **2007**, *7*, 3260–3265. Habenicht, B. F.; Kalugin, O. N.; Prezhdo, O. V. *Ab Initio* Study of Phonon-Induced Dephasing of Electronic Excitations in Narrow Graphene Nanoribbons. *Nano Lett.* **2008**, *8*, 2510–2516.
37. Valentin, A.; Sée, J.; Galdin-Retailleau, S.; Dollfus, P. Study of Phonon Modes in Silicon Nanocrystals Using the Adiabatic Bond Charge Model. *J. Phys.: Condens. Matter* **2008**, *20*, 145213-1–145213-8.
38. Lanzani, G.; Cerullo, G.; Zavelani-Rossi, M.; De Silvestri, S.; Comoretto, D.; Musso, G.; Dellepiane, G. Triplet-Exciton Generation Mechanism in a New Soluble (Red-Phase) Polydiacetylene. *Phys. Rev. Lett.* **2001**, *87*, 187402-1–187402-4.
39. Valenta, J.; Juhasz, R.; Linnros, J. Photoluminescence Spectroscopy of Single Silicon Quantum Dots. *Appl. Phys. Lett.* **2002**, *80*, 1070–1072.
40. Sychugov, I.; Juhasz, R.; Valenta, J.; Linnros, J. Narrow Luminescence Linewidth of a Silicon Quantum Dot. *Phys. Rev. Lett.* **2005**, *94*, 087405-1–087405-4.
41. Sykora, M.; Mangolini, L.; Schaller, R. D.; Kortshagen, U.; Jurbergs, D.; Klimov, V. I. Size-Dependent Intrinsic Radiative Decay of Rates of Silicon Nanocrystals at Large Confinement Energies. *Phys. Rev. Lett.* **2008**, *100*, 067401-1–067401-4.
42. Madelung, O.; Rössler U.; Schulz, M. *Group IV Elements, IV−IV and III−V Compounds: Semiconductors*; Springer-Verlag: Berlin and Heidelberg, 2001.
43. Talapin, D. V.; Murray, C. B. PbSe Nanocrystal Solids of n- and p-Channel Thin Film Field-Effect Transistors. *Science* **2005**, *310*, 86–89.
44. Yoffe, A. D. Low-Dimensional Systems: Quantum Size Effects and Electronic Properties of Semiconductor Microcrystallites (Zero-Dimensional Systems) and Some Quasi-Two-Dimensional Systems. *Adv. Phys.* **1993**, *42*, 173–266.
45. Wise, F. W. Lead Salt Quantum Dots: the Limit of Strong Quantum Confinement. *Acc. Chem. Res.* **2000**, *33*, 773–780.
46. Takagahara, T. Electron−Phonon Interactions in Semiconductor Nanocrystals. *J. Lumin.* **1996**, *70*, 129–143.
47. Schäfer, W.; Lövenich, R.; Fromer, N. A.; Chemla, D. S. From Coherently Excited Highly Correlated States to Incoherent Relaxation Processes in Semiconductors. *Phys. Rev. Lett.* **2001**, *86*, 344–347.
48. Creti, A.; Anni, M.; Rossi, M. Z.; Lanzani, G.; Manna, L.; Lomascolo, M. Role of Defect States on Auger Processes in Resonantly Pumped CdSe Nanorods. *Appl. Phys. Lett.* **2007**, *91*, 093106-1–093106-3.
49. Lupo, M. G.; Della, S. F.; Carbone, L.; Zavelani-Rossi, M.; Fiore, A.; Luer, L.; Polli, D.; Cingolani, R.; Manna, L.; Lanzani, G. Ultrafast Electron-Hole Dynamics in Core/Shell CdSe/CdS Dot/Rod Nanocrystals. *Nano Lett.* **2008**, *8*, 4582–4587.
50. Colonna, A. E.; Yang, X.; Scholes, G. D. Photon Echo Studies of Biexcitons and Coherences in Colloidal CdSe Quantum Dots. *Phys. Status Solidi B* **2005**, *242*, 990–1000.
51. Salvador, M. R.; Hines, M. A.; Scholes, G. D. Exciton-Bath Coupling and Inhomogeneous Broadening in the Optical Spectroscopy of Semiconductor Quantum Dots. *J. Chem. Phys.* **2003**, *118*, 9380–9388.
52. Paci, I.; Johnson, J. C.; Chen, X.; Rana, G.; Popovi, D.; David, D. E.; Nozik, A. J.; Ratner, M. A.; Michl, J. Single Fission for Dye-Sensitized Solar Cells: Can a Suitable Sensitizer Be Found? *J. Am. Chem. Soc.* **2006**, *128*, 16546–16553.
53. Klimov, V. I.; Ivanov, S. A.; Nanda, J.; Achermann, M.; Ilya, B.; McGuire, J. A.; Piryatinski, A. Single-Exciton Optical Gain in Semiconductor Nanocrystals. *Nature* **2007**, *447*, 441–446.
54. Prezhdo, O. V.; Rossky, P. J. Relationship between Quantum Decoherence Times and Solvation Dynamics in Condensed Phase Chemical Systems. *Phys. Rev. Lett.* **1998**, *81*, 5294-1–5294-4.
55. Skinner, J. L. Theory of Pure Dephasing in Crystals. *Annu. Rev. Phys. Chem.* **1988**, *39*, 463–478.
56. Kresse, G.; Furthmuller, J. Efficient Iterative Schemes for *Ab Initio* Total-Energy Calculations Using a Plane-Wave Basis Set. *Phys. Rev. B* **1996**, *54*, 11169. Kresse, G.; Hafner, J. *Ab Initio* Molecular Dynamics for Liquid Metals. *Phys. Rev. B* **1993**, *47*, 558–561. Kresse, G.; Hafner, J. Norm-Conserving and Ultrasoft Pseudopotentials for First-Row and Transition Elements. *J. Phys.: Condens. Matter* **1994**, *6*, 8245–8257. Vanderbilt, D. Soft Self-Consistent Pseudopotentials in a Generalized Eigenvalue Formalism. *Phys. Rev. B* **1990**, *41*, 7892–7895.
57. Perdew, J. P.; Chevary, J. A.; Vosko, S. H.; Jackson, K. A.; Pederson, M. R.; Singh, D. J.; Fiolhais, C. Atoms, Molecules, Solids, and Surfaces: Applications of the Generalized Gradient Approximation for Exchange and Correlation. *Phys. Rev. B* **1992**, *46*, 6671–6687.